Dynamics and Control of a Shuttle-Attached Antenna Experiment

Shyh Jong Wang,* Yu Hwan Lin,† and Che-Hang Charles Ih*
California Institute of Technology, Jet Propulsion Laboratory, Pasadena, California

Study results obtained to date identify the requirements for a large space system flight experiment. This paper considers the dynamics and control of an offset feed wrap-rib antenna attached to the Shuttle for such an experiment. Results reported herein are based primarily on the analysis and simulation of the combined Shuttle and antenna flexible dynamics model, and the Shuttle Vernier Reaction Control Subsystem. These results establish the technical feasibility of the Shuttle-attached antenna flight experiment. Static and dynamic disturbances examined do not cause significant dynamic interactions to the experiment. Shuttle vernier jets can be used for control purposes or as controlled excitation sources for experiment. Interface between the Shuttle and the antenna can be rigid or actively decoupled depending on the experiment objective. Key large space systems control technologies such as distributed sensing and actuation, system identification, figure estimation and control, and control for slew or reconfiguration can be validated with the experiment configuration described herein.

I. Introduction

FUTURE large space systems, such as the large space deployable antennas, present significant control problems due to unprecedented system size, variable flight configurations, and structural flexibility. These problems are further compounded with increasing system accuracy requirements. Large structure size and low mass density intensify the modeling problems. Mode shapes and modal frequencies no longer can be predicted accurately or measured at preflight time. Modern control technology at the present time cannot deal with large model uncertainties. In-flight system identification for initial model calibration and periodic alignment will be required for all large space system missions. Continuous system identification (ID) may be required for systems that require high performance or frequent configuration changes. A large number of packed modes at very low frequencies is a common property of large mesh deployable antennas. This considerably drives up the requirements of system ID algorithms, sensing, and processing capability from the state-of-the-art level. To deal with frequent configuration change and precision surface and pointing requirements, advanced distributed control, adaptive system ID and control, and figure determination and control systems will be required. All of these advanced systems are being developed but none have been applied to flight missions. Every new technology requires extensive test and evaluation before it can be applied for space missions. Uncertainties are so great that they can be reduced only by broadbase ground test and flight experiments.

The objective of the control flight experiment is to validate large space systems control technology for applicable future missions, such as large space antennas, manned space stations, multiple payload space platforms, segmented optical mirrors, etc. Specifically, the objectives of the flight experiments are 1) to establish large space systems control technology data base and reduce uncertainties in control and structure dynamic interactions; 2) to measure structural and system parameters (e.g., dampings) and their effects on open- and closed-loop dynamics; 3) to evaluate and validate critical control techniques, architectures, sensor and actuator hardware, and instrumentation for the control of large systems; and 4) to verify and establish a quantitative level of confidence and provide guidance for improvement of ground test, simulation, and tools of analytical prediction.

Control technology to be validated with the experiment includes system identification, precision pointing, vibration control, adaptive control, slew and configuration control, dynamic interaction and isolation control, and shape determination and control.

A large space antenna attached to the Space Shuttle provides an excellent flight experiment opportunity for both the space station and the large space antenna. The reason is that the Space Shuttle can be considered as a first-order space station and the attached antenna as its flexible payload. Conversely, the Space Shuttle can be considered as a rigid spacecraft bus and feed attached to a flexible large space antenna operated as a free-flier. System ID can be performed for the flexible reflector and its supporting boom structure. Control during antenna deployment or slew provides adaptive control or slew control experiment opportunity. The interface between antenna boom and the Shuttle can be used to test interaction and isolation control.

This paper focuses on the presentation of technical feasibility results, with particular emphasis on Shuttle and antenna dynamic interactions, compatibility of the Shuttle control system, and Shuttle and antenna stability with added proportional control. Feasibility results are obtained with applications of modern analysis techniques and simulations. A new hardware concept for the isolation and decoupling between the Shuttle and the antenna is proposed. Other works related to the flight experiment are presented in Refs. 1 and 2.

II. Configurations and Mass Properties

A. Configurations of Shuttle and Antenna

The antenna configuration studied is the 55 mD wrap-rib deployable antenna.[3] The Space Shuttle configuration and properties employed herein are those of the Columbia Orbiter for flight No. 3.[4] Figure 1 illustrates the free-flier antenna and three attachment configurations. The rigidly attached system has the advantage of structural and dynamic similarity to a free-flier antenna. The gimbal-attached configuration offers

Presented as Paper 83-2227 at the AIAA Guidance and Control Conference, Gatlinburg, Tenn., Aug. 15-17, 1983; submitted March 19, 1984; revision received June 19, 1984.

*Member of Technical Staff, Automation and Energy Systems Division. Member AIAA.

†Member of Technical Staff, Automation and Energy Systems Division.

the option of slew operation and dynamical decoupling of the antenna and Shuttle. The bus-attached system is similar to platform applications but its dynamical properties are different from those of free-fliers. In this paper, the discussions are focused largely on the rigidly feed-attached configuration, although some considerations of the controlled decoupled configuration are discussed in a later section.

B. Mass Properties

The mass of the Shuttle and the antenna is 102,788.73 kg (226,135.2 lb). The shift of center of mass (c.m.) from the Shuttle c.m. is noted as follows:

$$\Delta x = 0.045 \text{ m } (1.77 \text{ in.})$$

$$\Delta y = 0$$

$$\Delta z = -0.392 \text{ m } (-15.44 \text{ in.})$$

For control and dynamic analysis, the body coordinates, X_B, Y_B, Z_B, are used (see Figs. 2 and 3).

The moment of inertia matrix for the combined system is approximately

$$I = \begin{bmatrix} 4.464\times10^6 & 0 & -3.891\times10^5 \\ 0 & 13.270\times10^6 & 0 \\ -3.891\times10^5 & 0 & 10.706\times10^6 \end{bmatrix} \text{kg-m}^2$$

It can be shown that the body frame and the principal axes differ by an angle of -3.96 deg about the Y_B axis.

It is noted that although the antenna is extremely light in mass compared with that of the Shuttle, the moment of inertia about the X axis of the combined system has greatly increased from that of the Shuttle.

III. Dynamic Equations of the Shuttle-Attached Antenna System

The modeling approach for the Shuttle-attached antenna system follows that reported in Ref. 5, and is briefly described herein for quick reference. The equations of motion are obtained using Lagrange's formulation

$$\frac{d}{dt}(\nabla_{\dot{x}} L) - \nabla_x L = F$$

where $\nabla_{\dot{x}}$ and ∇_x are the gradients with respect to the generalized velocities and positions, respectively; L is the Lagrangian defined by

$$L = T - V$$

where T is the kinetic energy of the system, and V the potential energy of the system. F is the sum of all nonconservative forces applied to the system.

The total kinetic (T) and potential (V) energy of the system are obtained by considering the system as being composed of three bodies, i.e., flexible antenna dish, flexible boom structure, and rigid Shuttle.

The flexible antenna was modeled by a finite element model[6] with 6624 nodes. Six significant modes of this model were chosen representing the dish kinetic and potential energy. The flexible boom was modeled with a three-degree-of-freedom hinge, representing the first three modes associated with the L-shaped boom structure. Similarly, the kinetic and potential energy of the boom were expressed in terms of these three modes. Finally, the Shuttle is treated as rigid and, therefore, it contributes only kinetic energy to the overall system.

As the kinetic and potential energy of the system are substituted into the Lagrange's formulation, and all the derivatives and gradients are performed, the following equation results:

$$M\ddot{x} + Kx = F$$

where $x = (\phi, \theta, \psi, \gamma_1, \gamma_2, \gamma_3, q_1, \ldots, q_6)^T$ is the state of the system, and ϕ, θ, and ψ are the roll, pitch, and yaw attitude angles of the Shuttle, respectively; γ_1, γ_2, and γ_3 are the three hinge angles relative to the angles at rest; $q_1, \ldots, q_6$ are the six modal amplitudes of the dish.

M and K are the 12×12 mass and stiffness matrices, and F is the torque and force vector applied to the system. Let

$$M = \begin{bmatrix} M_{\theta\theta} & M_{\theta\gamma} & M_{\theta q} \\ & M_{\gamma\gamma} & M_{\gamma q} \\ (\text{Symm}) & & M_{qq} \end{bmatrix}$$

and

$$K = \begin{bmatrix} 0 & 0 & 0 \\ & K_{\gamma\gamma} & 0 \\ (\text{Symm}) & & K_{qq} \end{bmatrix}$$

Table 1 Modal frequencies for the 55-mD antenna configurations, Hz

Mode no.	Free-flier	Shuttle attached	Mode shape description
1	0	0	
2	0	0	Rigid body modes
3	0	0	
4	0.0874844	0.0611325	Short boom torsion and dish rotation
5	0.149257	0.0934743	Dish torsion and long boom twist
6	0.182630	0.176617	Dish torsion and long boom bending
7	0.211687	0.195617	Dish bending
8	0.228549	0.201674	Dish and long boom bending
9	0.425039	0.249602	Dish torsion and warping
10	0.757510	0.749665	Dish rotation
11	0.968000	0.990986	Dish cupping and long boom bending
12	1.53375	1.558930	Dish torsion and warping

Table 2 Gravity gradient torque at norminal nadir attitude

Altitude h, km	200	300	400	600	800	1000
$-Tgy$, N-m	1.634	1.562	1.494	1.369	1.245	1.131
$-Tgy$, ft-lb	1.206	1.152	1.102	1.010	.918	8.35

Table 3 Gravity gradient and gyroscopic torques at nominal nadir attitude

h, km	200	300	400	600	800	1000
$-Tggy$, N-m	2.179	2.083	1.992	1.825	1.660	1.508
$-Tggy$, ft-lb	1.608	1.536	1.469	1.347	1.224	1.113

The values for M and K are

$$M_{\theta\theta}=\begin{bmatrix} 4.52E6 & -4.69E3 & 1.24E5 \\ & 1.33E7 & -3.32E3 \\ (\text{Symm}) & & 1.07E7 \end{bmatrix} \qquad M_{\gamma\gamma}=\begin{bmatrix} 5.45E4 & 0 & -1.04E4 \\ & 5.06E5 & 0 \\ (\text{Symm}) & & 5.59E5 \end{bmatrix}$$

$$M_{qq}=\begin{bmatrix} 1 & 0 & 0 & 0 & 0 & 0 \\ & 0.999 & 0 & 0 & 0 & 0.0001 \\ & & 0.999 & 0 & -0.0001 & 0 \\ & & & 0.998 & 0 & 0 \\ (\text{Symm}) & & & & 1.000 & 0 \\ & & & & & 1.000 \end{bmatrix} \qquad M_{\theta\gamma}=\begin{bmatrix} 2.83E4 & 0 & 1.14E6 \\ 0 & 2.38E5 & 0 \\ -4.90E3 & 0 & 3.18E5 \end{bmatrix}$$

$$M_{\theta q}=\begin{bmatrix} 0 & 1.06E2 & 8.03E2 & 0 & -1.26E2 & 1.66E1 \\ -1.83E-3 & -8.03E2 & 1.06E2 & -1.85E2 & -1.66E1 & -1.26E2 \\ 3.13E2 & 1.87E1 & 1.42E2 & 3.00E-4 & 1.32E1 & -1.73E0 \end{bmatrix}$$

$$M_{\gamma q}=\begin{bmatrix} 0 & -1.86E0 & -1.41E1 & 0 & -2.02E2 & 2.66E1 \\ -4.06E-3 & 1.41E1 & -1.86E0 & -4.09E2 & -2.66E1 & -2.02E2 \\ 3.13E2 & 4.13E1 & 3.14E2 & 3.00E-4 & 2.93E1 & -3.84E0 \end{bmatrix}$$

$K_{\gamma\gamma}=\text{diag}(1.8366E4, 6.3766E5, 4.1900E4)$

$K_{qq}=\text{diag}(1.3058, 1.4209, 1.4209, 22.1624, 22.1794, 22.1794)$

To simplify the solution, an eigenvalue problem was solved. Let $x=\Phi z$, where Φ is the generalized eigenvector matrix. The new decoupled dynamic equations, after adding damping terms, are

$$\ddot{z}_k=\phi_k^T F \qquad k=1,2,3$$

$$\ddot{z}_k+2\zeta_k\omega_k\dot{z}_k+\omega_k^2 z_k=\phi_k^T F \qquad k=4,\dots,12$$

where the modal frequencies $(\omega k/2\pi)$, $k=4,\dots,12$ are shown in Table 1.

As the damping is added, the corresponding equations of motion in physical coordinates should read

$$M\ddot{x}+D\dot{x}+Kx=F$$

where D is as follows:

$$D=\Phi^{-T}\text{diag}(2\zeta_k\omega_k)\Phi^{-1}$$

IV. Environmental Disturbances

A. Orbital Configuration

Referring to Fig. 3, the nominal orbit is assumed to be at 400 km altitude and circular. The Shuttle is oriented for nadir with the body Z_B axis pointing toward the center of the Earth.

B. Gravity Gradient Torque Estimates

Let Tg be the gravity gradient torque vector, ω_0 the orbital angular rate, and u_R the unit Earth vector (pointing toward the Shuttle from the center of the Earth). For circular orbits,

$$Tg=3\omega_0^2\tilde{u}_R I u_R)$$

For $u_R=(0\ 0\ -1)^T$, I given in Sec. II.B, and $\tilde{u}_R$, the skew symmetric matrix for u_R,

$$Tg=\begin{bmatrix} 0 \\ -1.167\times 10^6 \\ 0 \end{bmatrix}\omega_0^2$$

For the nominal altitude, $h=h_0=400$ km and $\omega_0=0.0011315$ rad/s,

$$Tg=Tg_{h_0}=\begin{bmatrix} 0 \\ -1.494 \\ 0 \end{bmatrix}\text{N-m}$$

For some other altitude h,

$$Tg_h=\left(\frac{6378.2+h_0}{6378.2+h}\right)^3 Tg_{h_0}$$

where h and h_0 are in km and Tg is in N-m.

Table 2 shows the gravity gradient torque for various altitudes.

C. Gyroscopic Torque Estimates

Since the nominal attitude of the Shuttle is assumed to be nadir with the body z_B axis (rather than the principal z_p axis) pointing to Earth, there is a nonzero gyroscopic torque about the y_B axis. Table 3 shows the sum of the gravity gradient torque and the gyroscopic torque.

D. Atmospheric Drag Torque Estimates

The atmospheric drag force may be estimated by using the following equation:

$$F=\tfrac{1}{2}C_D A\rho v^2$$

where A is the cross-sectional area of the Shuttle opposing the direction of motion, ρ the air density, v the orbital velocity, and C_D the dimensionless drag coefficient. The value of C_D is a function of the shape of the Shuttle and the flow regime. In Ref. 7, the values of C_D between 1 and 2 have been stated. Values between 2.5 and 3.0 have been suggested in Ref. 8 for large deployable antennas. The value of 2.75 is used in this paper.

The air densities ρ corresponding to the 97.7 percentile values for the solar flux numbers and the geomagnetic index were obtained for three orbital altitudes: 250, 300, and 400 km. The current solar activity has a cyclic period of about eight years with a low in 1986. The 1986 density has been used here and the values for the three altitudes are 0.0702, 0.0206, and 0.00241 kg/km^3, respectively. The estimated area for the antenna structure is 86.37 m^2 (929.66 ft^2) and the center of pressure (c.p.) is approximately 55.53 m above the Shuttle c.m. The cross-sectional area of the Shuttle is 64.1 m^2 (690 ft^2) (obtained from Ref. 9), and the estimated c.p. is 0.938 m below the Shuttle c.m. Table 4 shows the estimated atmospheric forces and torques of the Shuttle and antenna.

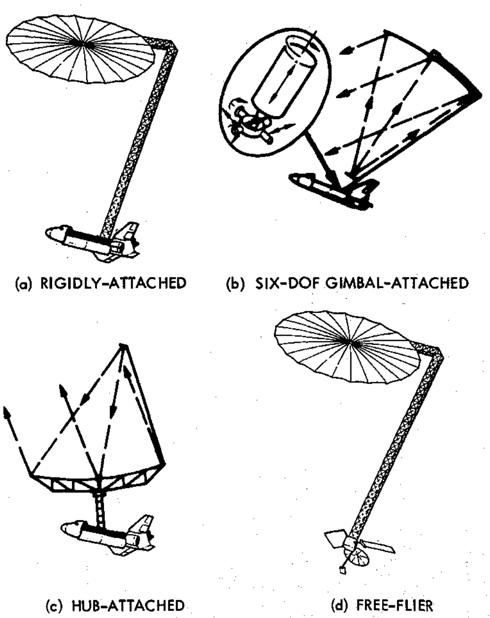

Fig. 1 Flight experiment configurations.

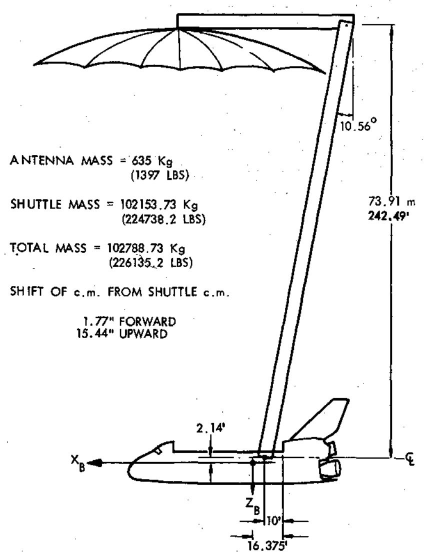

Fig. 2 Shuttle-attached antenna flight experiment configuration.

E. Attitudes for Zero Nominal Disturbance Torques

So far the gravity gradient torque, the gyroscopic torque, and the atmospheric drag torque at the nominal pointing attitude have been estimated. No estimate has been made for the solar pressure torque. This disturbance has been omitted because, at the low-Earth orbits, it is at least one order of magnitude less than other disturbances. Figure 4 shows the torques as a function of altitude. Note that, from Fig. 4, the drag torque and other torques have opposite signs. For a given altitude, these torques may cancel each other by properly selecting the attitude angle. Let θ be the attitude angle about the y_B axis. Referring to Fig. 5, the unit Earth

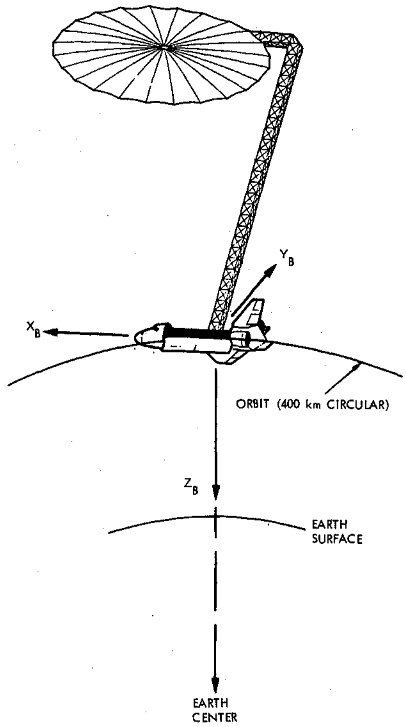

Fig. 3 Orbital configuration.

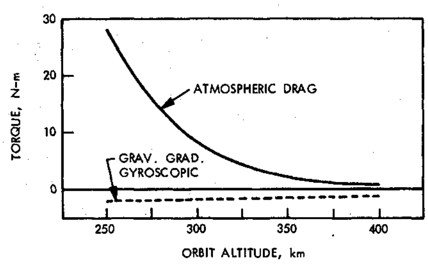

Fig. 4 Estimated disturbance torques for the Shuttle and experiment.

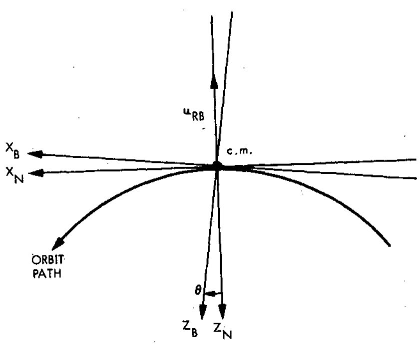

Fig. 5 Zero disturbance attitude.

vector in body frame u_{RB} is

$$u_{RB} = \begin{bmatrix} \sin\theta \\ 0 \\ -\cos\theta \end{bmatrix}$$

The gravity gradient and gyroscopic torque at this attitude are

$$Tgg = \frac{4}{3}\,(3\omega_0^2 \tilde{u}_{RB} I u_{RB})$$

$$= -1.556\times 10^6 \omega_0^2 \begin{bmatrix} 0 \\ \cos 2\theta - 8.021\sin 2\theta \\ 0 \end{bmatrix}$$

The only nonzero component is

$$Tggy = -1.556\times 10^6 \omega_0^2 (\cos 2\theta - 8.021\sin 2\theta)$$

Let T_{dy} be the drag torque. To determine θ for zero disturbance, setting $T_{ggy} + T_{dy} = 0$, and solving for θ, one has

$$\theta = \frac{1}{2}\left[7.1066\ \text{deg} - \sin^{-1}\left(\frac{7.949\times 10^{-8} T_{dy}}{\omega_0^2}\right)\right]$$

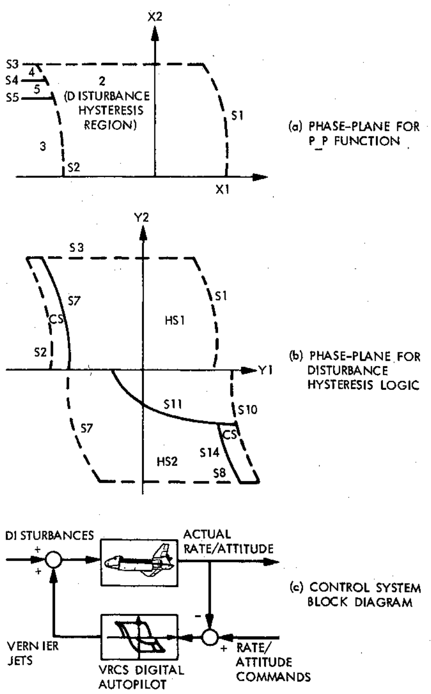

Fig. 6 Shuttle Vernier Control Subsystem.

For $h=250$ km, $\omega_0 = 1.17013\times 10^{-3}$ rad/s, it can be shown that there is no real solution for θ. For $h=300$ km, $\omega_0 = 1.15701\times 10^{-3}$ rad/s, $\theta = -9.68$ deg. For $h=400$ km, $\omega_0 = 1.1315\times 10^{-3}$ rad/s, $\theta = 2.01$ deg.

V. Shuttle Vernier Reaction Control Subsystem (VRCS)

The Shuttle Reaction Control Subsystem (RCS) consists of two systems, the primary and the vernier systems.[10,11] The primary system provides ΔV changes, attitude maneuvers, and gross attitude control functions; and the VRCS provides the fine attitude control functions. Figure 6 shows the VRCS phase-plane control system. The coordinate axes in Fig. 6 are defined as follows:

$$X_1 = \text{sign}(\omega_e)\theta_e, \qquad X_2 = |\omega_e|$$

$$Y_1 = \text{sign}(U_D)\theta_e, \qquad Y_2 = \text{sign}\,(U_D)\omega_e$$

where θ_e and ω_e are the attitude error and the attitude rate error, respectively, and U_D is the undesirable acceleration. The other phase-plane definitions can be found in Ref. 11.

The phase-plane attitude deadband (DB) has a selectable range of 0.01 to 40 deg and a minimum rate limit (RL) of 0.01 deg/s. Typical deadband and rate limit are 0.01 deg – 1.0 deg and 0.02 deg/s, respectively.

The VRCS employs six hydrazine gas jets of 24 lbs of thrust each. These jets have a specific impulse of 228 s with two of the jets located at the forward Shuttle section and four at the aft section.

Figure 7 shows the simulated limit cycle characteristics of the Shuttle for various deadbands, rate limits, and initial conditions. A limit cycle period of longer than 8 min appears achievable for even moderately tight phase-plane parameter values.

Table 4 Estimated atmospheric drag for the Shuttle and experiment

Altitude, km	Force, $-Fx$, N	Torque, Ty, N-m
250	0.876	27.58
300	0.253	7.96
400	0.029	0.92

Table 5 List of simulation cases

	VRCS	HRWC	BCMGC	Comments
1	off	off	off	Open-loop simulation
2	on	off	off	Bang-Bang control only
3	off	on	off	Proportional control only
4	on	on	off	Bang-Bang and proportional control
5	off	on	on	Two-site proportional control

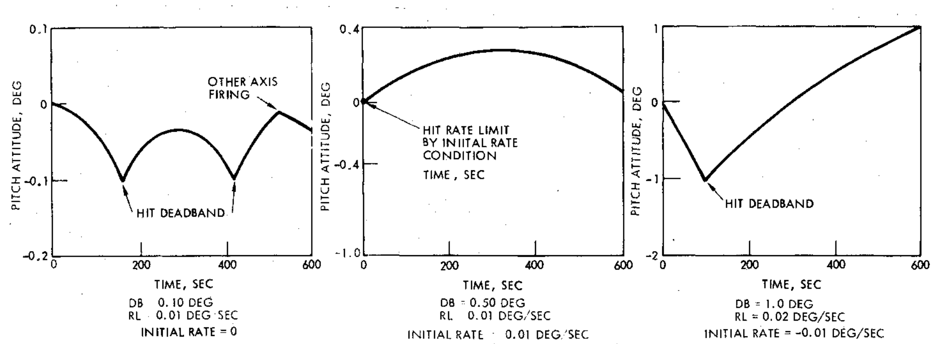

Fig. 7 Simulated VRCS limit cycles (Shuttle OV-102).

VI. Dynamics and Control Simulations

A. Simulated Cases for the Shuttle-Attached Antenna Experiment

To explore various control possibilities for the experiment configuration, three controllers are selected for simulation studies: the Shuttle VRCS as discussed in Sec. V, the Hub Reaction Wheel Control (HRWC), and the Bay Control Moment Gyro Control (BCMGC).

HRWC consists of three reaction wheels mounted at the hub of the dish providing three-axis rotational control of the entire dish.[3] The torque level requirement of these wheels is less than 2 N-m.

The BCMGC consists of one or more CMG's located at the Shuttle payload bay near the attachment interface. Up to a 200 N-m torque level is required for the BCMGC, which is implemented in the simulation to quantify its performance improvement over the Shuttle VRCS.

Table 5 tabulates the cases for which simulation results have been obtained.

As the Hub or CMG controls are employed, the closed-loop system equation becomes

$$M\ddot{x}+D\dot{x}+Kx=Bu+Bw$$

where M, D, K, and x are the same as defined in Sec. III; B is the 12×12 control influence matrix; the position plus rate feedback control vector u is

$$u=-C_I x-C_2\dot{x}$$

and w is the system disturbance vector. The values of the B matrix elements are defined as follows. Let B be denoted by

$$B=\begin{bmatrix} B_{T0\theta} & B_{TI\theta} & B_{F\theta} \\ 0 & B_{TI\gamma} & B_{F\gamma} \\ 0 & 0 & B_{Fq} \end{bmatrix}$$

where the values for B_{ij} are

The position control gain matrix C_I is

$$C_I=\begin{bmatrix} C_{I\theta\theta} & 0 & 0 \\ & C_{I\gamma\gamma} & 0 \\ \text{(Symm)} & & 0 \end{bmatrix}$$

the values for C_{Iij} are

$$C_{I\theta\theta}=\text{diag}(7.5E4,\ 36.0E4,\ 22.0E4)$$

$$C_{I\gamma\gamma}=\text{diag}(139.0,\ 1392.0,\ 772.0)$$

The rate control gain matrix C_2 is

$$C_2=\begin{bmatrix} C_{2\theta\theta} & 0 & 0 \\ & C_{2\gamma\gamma} & 0 \\ \text{(Symm)} & & 0 \end{bmatrix}$$

the values for C_{2ij} are

$$C_{2\theta\theta}=\text{diag}(75.0E5,\ 360.0E5,\ 220.0E5)$$

$$C_{2\gamma\gamma}=\text{diag}(1112.0,\ 11138.0,\ 6173.0)$$

Three types of disturbances (w) have been considered: 1) environmental disturbance torques as discussed in Sec. IV, 2) preprogrammed two-pulse Shuttle VRCS jet firings, and 3) preprogrammed repetitive Shuttle VRCS jet firings.

The two-pulse preprogrammed sequence is that at time = 0 turn off VRCS for 5 s and burn Vernier Thruster R5D for 0.48 s and at time = 3.52 s burn Vernier Thruster L5D for 0.48 s.

The preprogrammed repetitive Vernier Thruster burns are as follows: at time = 0 burn Thruster R5D for 0.40 s, at time = 5 s burn Thruster L5D for 0.40 s, at time = 10 s burn

$$B_{T0\theta}=\begin{bmatrix} 1 & 0 & 0 \\ 0 & 1 & 0 \\ 0 & 0 & 1 \end{bmatrix}\quad B_{TI\theta}=\begin{bmatrix} 1 & 0 & 0 \\ 0 & 1 & 0 \\ 0 & 0 & 1 \end{bmatrix}\quad B_{TI\gamma}=\begin{bmatrix} 1 & 0 & 0 \\ 0 & 0.98 & -0.18 \\ 0 & 0.18 & 0.98 \end{bmatrix}$$

$$B_{F\theta}=\begin{bmatrix} 0 & -0.39 & 0 & 0 & 74.13 & 0 \\ 0.39 & 0 & 0.07 & -74.13 & 0 & -13.96 \\ 0 & -0.07 & 0 & 0 & 13.96 & 0 \end{bmatrix}$$

$$B_{F\gamma}=\begin{bmatrix} 0 & 0.34E-2 & 0 & 0 & -0.05 & 0 \\ -0.34E-2 & 0.03 & 0.15 & 0.05 & -5.42 & -29.09 \\ -0.63E-3 & -0.15 & 0.03 & 0.85 & 29.09 & -5.42 \end{bmatrix}$$

$$B_{Fq}=\begin{bmatrix} 0 & 0 & 0 & 0 & 0 & 0 \\ 0 & 0 & 0 & 0.11E-3 & 0.14E-4 & -0.26E-4 \\ 0 & 0 & 0 & 0.14E-4 & 0.11E-3 & -0.20E-4 \\ 0 & 0 & 0 & 0 & 0.26E-4 & 0.14E-3 \\ 0 & 0 & 0 & 0.13E-5 & 0.98E-5 & -0.18E-5 \\ 0 & 0 & 0 & -0.10E-4 & 0.13E-5 & -0.24E-6 \end{bmatrix}$$

Thruster F5L for 0.40 s, and at time = 15 s burn Thruster F5R for 0.40 s and repeat the above every 60 s.

B. Numerical Results

Selective simulation results are discussed in the following paragraphs, and illustrated in Figs. 8-13.

Figure 8 assumes the condition of VRCS on, Hub Control on or off, and BCMGC off. It shows a Shuttle pitch limit cycling behavior, as the experiment configuration is subject to the environmental disturbance. There is no marked difference in this behavior between the Hub Control on and off. However, as the results of Fig. 8 are compared with that of Fig. 7 for the Shuttle without the antenna, it is found that the limit cycle period for the experiment configuration extends longer for the same selected VRCS deadband and rate limit. This results from the increased moment of inertia and the decreased net disturbance torque for the experiment configuration.

Figure 9 shows dish-to-Shuttle relative attitude response under the condition specified for Fig. 8. The results indicate that there is no relative dish attitude error for the first 200 s of the simulation until the Shuttle attitude reaches the phase-plane switching line and the VRCS jets get turned on. As shown in the figure, the peak error is smaller and damped faster when the Hub Control is on, since the controller has increased the damping and stiffness to the system.

Results in both Figs. 10 and 11 have been obtained with two-pulse preprogrammed jet firings at the beginning of the simulation. The Shuttle limit cycle behavior indicated in Fig. 10 still confirms that an eight-minute limit cycle period is achievable even with preprogrammed jet firing disturbances. Figure 11 indicates that the Hub Control has not significantly improved the dish boresight error (a combination of the Shuttle attitude error and the relative dish attitude error). However, the Hub control is very effective in reducing the dish-to-Shuttle relative attitude error.

Results shown in Fig. 12 are obtained under the preprogrammed repetitive Vernier jet firing disturbances with the VRCS control disabled. It has demonstrated in the figure that the dish surface accuracy has improved by a factor of 2

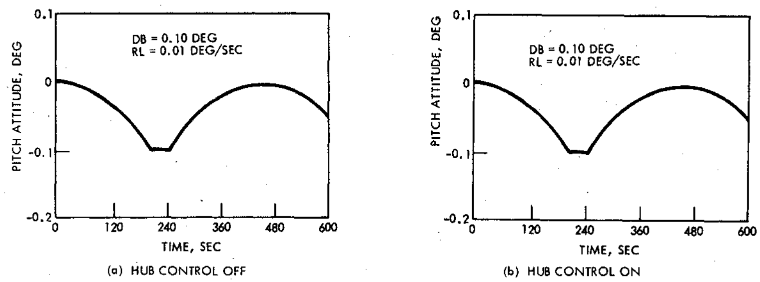

Fig. 8 Pitch attitude limit cycles with antenna attached.

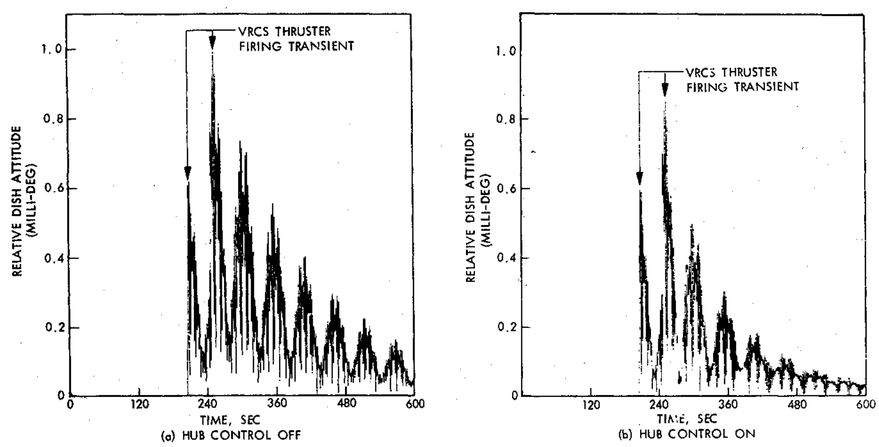

Fig. 9 Relative dish attitude response to VRCS jet firings.

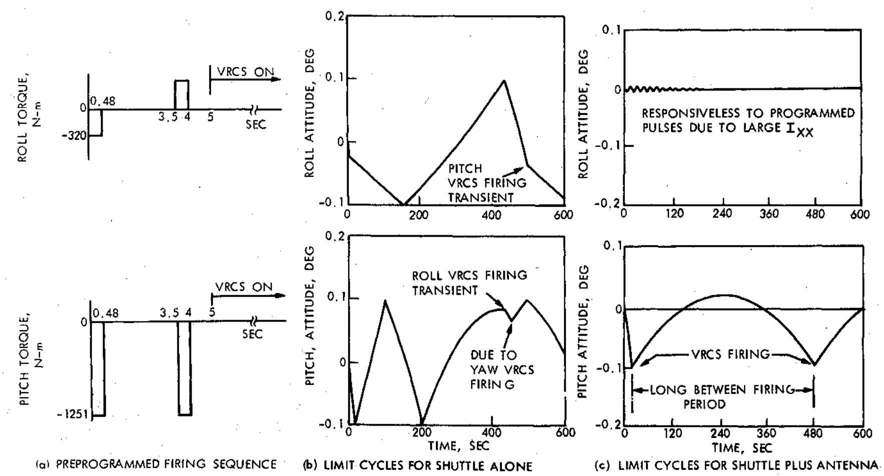

Fig. 10 Limit cycles under preprogrammed jet firings.

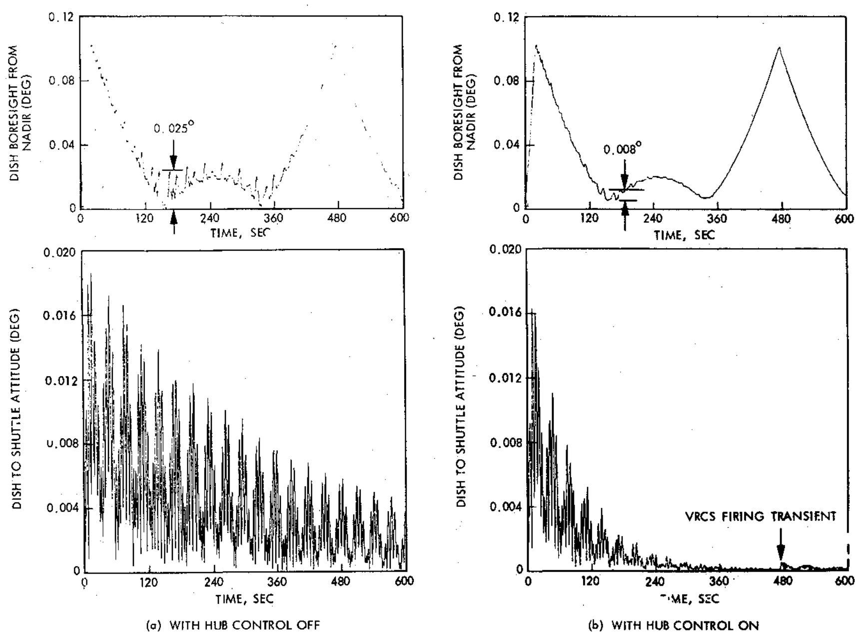

Fig. 11 Simulated limit cycles under preprogrammed thruster firings.

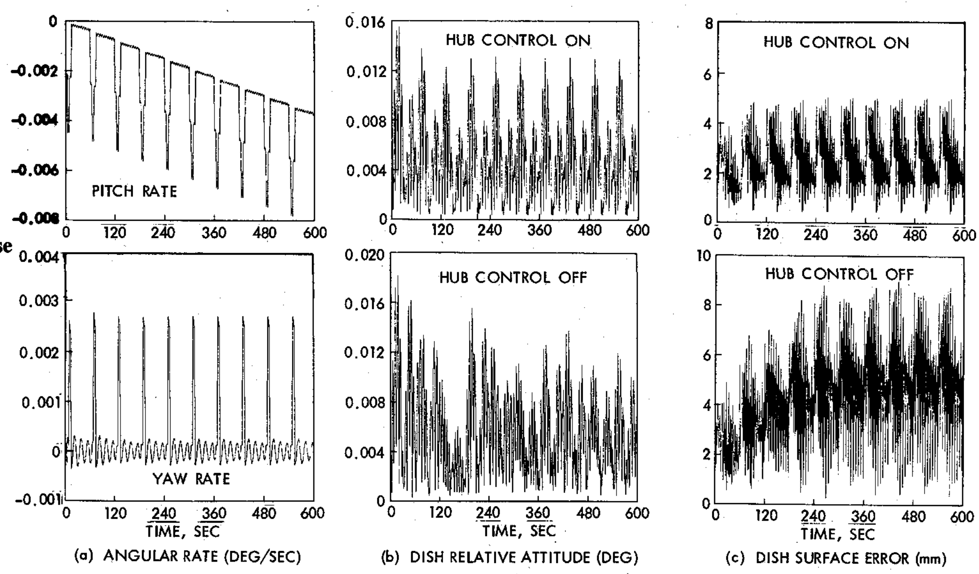

Fig. 12 Shuttle plus antenna response under preprogrammed thruster firings.

with the Hub Control on. It is also quite noticeable that with the Hub Control on the response shows regularity.

Figure 13 shows that with Hub Control and the Shuttle payload bay CMG Control activated and the Shuttle VRCS deactivated, the experiment configuration can be controlled to minimize system errors.

VII. A Six-Degree-of-Freedom Controlled Attachment Interface System

To provide a broad spectrum of large system flight experiment, a 6-dof (three rotations and three translations) controlled interface system is proposed. A conceptual model of this system is illustrated in Fig. 14. Basically, this interface system is mounted in the Shuttle payload bay near the c.m. The system has its own sensing and control mechanisms which are capable of following the antenna boom tip motion without touching the boom structure during the free-flier experiment.

The operation of this interface is briefly discussed as follows. First, the boom tip is attached to the inner axis of the interface. After the Shuttle is inserted into its orbit and at the desired attitude, the antenna structure will be erected with the gimbal control of the interface. Upon completion of the antenna deployment, the boom tip will be uncaged and tracked by the system through a 1-m sphere of motion. Between the boom tip and the inner axis assembly of the interface system, there is a 6-dof sensing system which provides intelligence for the interface controller to track the boom position. After the system reaches the 1-m sphere tracking boundary, the interface sensing system will provide positional information to derive antenna station keeping data needed to reposition the antenna and, hence, the interface to their starting position. Once respositioned, the free-drift mode of operation can be initiated. In this mode of operation the antenna and Shuttle are separate inertial entities in which the antenna is a free structure flying in tight formation with the Shuttle, with 1 cm separation from the inner structure of the 6-dof tracker controller. It is important to note that in order to obtain long free-drift periods, one has to place the antenna c.m. co-orbital with the Shuttle c.m. For this purpose, it is necessary for the Shuttle to fly in the nosedown nadir attitude.

A realizable flight experiment architecture is illustrated in Fig. 15. As all of the six axes of the interface are frozen,

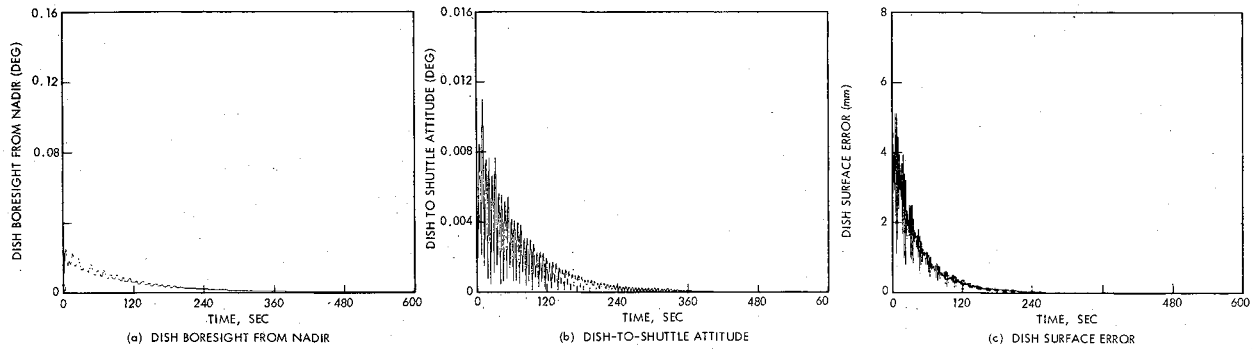

Fig. 13 System response with payload bay CMG and Hub Controls activated and VRCS deactivated.

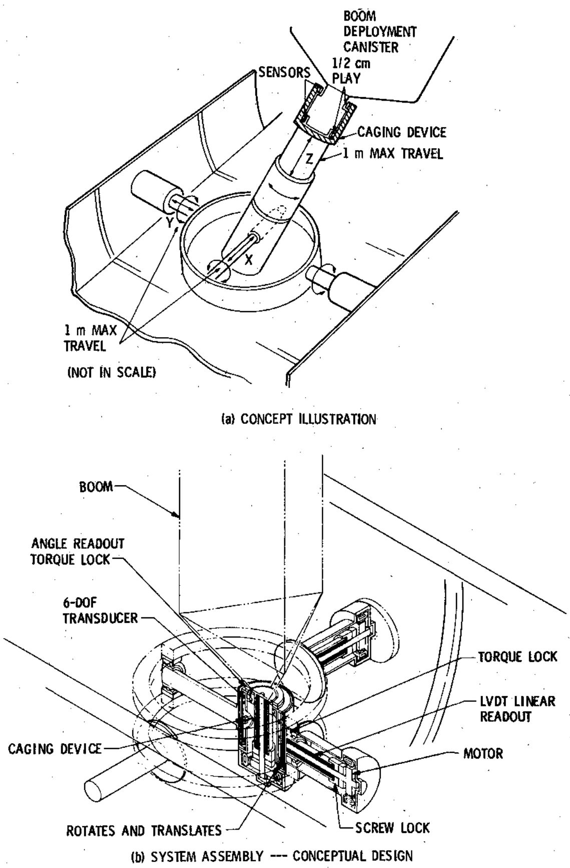

Fig. 14 Six-DOF Controlled Attachment Interface System.

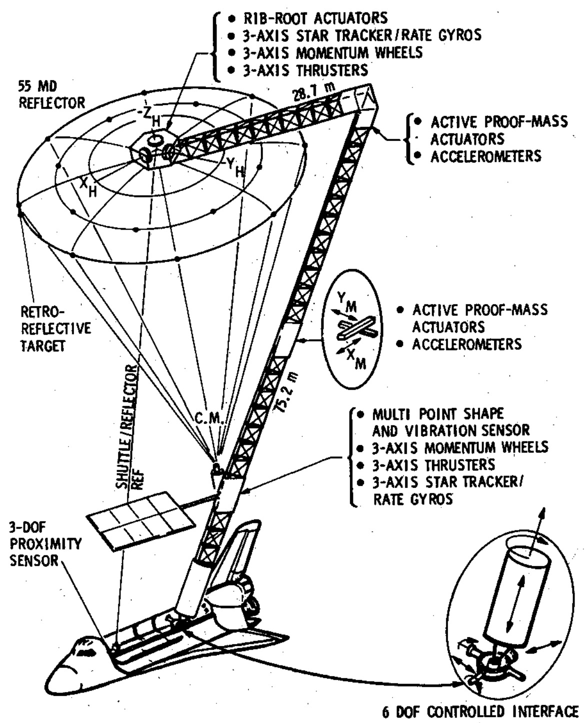

Fig. 15 Flight experiment architecture.

the configuration shown in Fig. 15 becomes that of the rigidly attached configuration of Fig. 1. However, the 6-dof interface system provides significant improvement in safety and stability to the experiment configuration; and at the same time, allows graceful antenna erection, slew, reconfiguration, disturbance isolation between Shuttle and antenna, and the possibility for a simulated free-flying antenna experiment.

VIII. Summary of Findings

1) The antenna significantly increases the moment of inertia of the Shuttle, but it changes the center of mass only slightly.

2) At the nominal altitude of 400 km, the atmospheric drag forces and torques do not seem to impact the control experiment significantly. The estimated drag torques, at this altitude, are on the order of 1 N-m and the gravity gradient and gyroscopic torques are approximately 1.5 N-m. The net disturbance torque is approximately 0.5 N-m. The net disturbance for the Shuttle alone is about 1.4 N-m.

3) Mass properties and disturbance torques dominate the limit-cycle behavior for a given deadband angle and rate limit. The antenna structural vibrations have no significant effects on the limit cycles.

4) Limit cycle periods of 8 min can be achieved under favorable conditions—even for a set of tight phase-plane parameters, e.g., deadband of 0.5 deg and rate limit of 0.01 deg/s. With this limit cycle rate, control experiments conceived to date could be conducted.

5) The simulated antenna structure is stable either with or without the Hub Control turned on. However, the Hub Control adds more damping to the otherwise very vibratory structural dynamics. The above is true whether the structure is under the influence of the Vernier Reaction Control Subsystem or various preprogrammed Vernier thruster firing sequences.

6) The Shuttle payload bay CMG control and the Hub Control further demonstrate pointing improvement and high stability for distributed control systems.

7) The 6-dof Controlled Attachment Interface System is invaluable to the experiment.

IX. Conclusions

1) The Space Shuttle-Attached Large Space Antenna Control Experiments do not require alternations of the existing Vernier Reaction Control Subsytem.

2) Most of the control experiments conceived to date can be performed during the quiescent period between thruster firings. The length of the quiescent period can be prolonged by increasing the deadband and the rate limit of the phase-plane control law.

3) The antenna structural vibration does not contribute significantly to the Orbiter and antenna dynamic interactions, hence it poses no hazard to the Orbiter during the experiment.

4) The atmospheric drag at the 400-km altitude level is not large enough to be hazardous to the experiment. By slightly tilting the Orbiter about the orbit normal, the drag torque and the gravity gradient torque can be balanced, which, in turn, will reduce the limit cycle rate.

5) The proposed Shuttle-attached antenna flight experiment is tehnically feasible.

Acknowledgments

The authors would like to thank J.M. Cameron, M. Hamidi, and G.S. Perkins for their contributions to this work.

This research was carried out by the Jet Propulsion Laboratory, California Institute of Technology, under contract with the National Aeronautics and Space Administration.

References

[1] Rodriguez, G., Hamidi, M., and Eldred, D., "Maximum Likelihood Identification of Parameters in Static and Dynamic Shape Estimator Models," *4th VPI&SU/AIAA Symposium on Dynamics and Control of Large Structures,* Blacksburg, Va., June 1983, pp. 497-524.

[2] Milman, M.H., Scheid, R.E. Jr., Cameron, J.M., Rodriguez, G., "Static Shape Determination for Large Structures," *4th VPI&SU/AIAA Symposium on Dynamics and Control of Large Structures,* Blacksburg, Va., June 1983, pp. 239-264.

[3] Cameron, J.C., Hamidi, M., Lin, Y.H., and Wang, S.J., "Distributed Control of Large Space Antennas," NASA/JPL Workshop on Applications of Distributed System Theory to the Control of Large Space Structures, June 1982.

[4] *Shuttle Operational Data Book,* JSC-08934, Vol. II, Rev. B, Aug. 1980; Amendment 46, Jan. 6, 1982.

[5] Hamidi, M., Rodriguez, G., and Schaechter, D.B., "Distributed System Modeling of a Large Space Antenna," NASA/JPL Workshop on Applications of Distributed System Theory to the Control of Large Space Structures, July 1982.

[6] El-Raheb, M. and Wagner, P., "Static and Dynamic Characteristics of Large Deployable Space Reflectors," AIAA Paper 81-0503, April 1981.

[7] Wertz, J.R., ed., *Spacecraft Attitude Determination and Control,* D. Reidel Publishing Co., Boston, Mass, 1978.

[8] Beach, S.W., "General Considerations of Control Disturbances for Large Space Structures," Final Report prepared for JPL, Jan. 18, 1980.

[9] *Space Transportation System User Handbook,* NASA N77-82346, June 1977.

[10] Blevins, D.R. and Hohmann, C.W., "Description of the Space Shuttle Reaction Control System," AIAA Paper 75-1299, Oct. 1975.

[11] "Space Shuttle Orbiter Orbital Flight Test, Level C, Functional Subsystem Software Requirements, Guidance, Navigation, and Control, Part C, Flight Control, Part 2," SD 76-SH-0009 Book 2B, Sept. 15, 1980.